Singular analysis of Fano resonances in plasmonic nanostructures

V. Grigoriev,[*] S. Varault, G. Boudarham, B. Stout, J. Wenger, and N. Bonod

CNRS, Aix Marseille Université, Centrale Marseille, Institut Fresnel, UMR 7249, 13013 Marseille, France

The scattering properties of plasmonic nanostructures arranged in two-dimensional periodic arrays are analyzed by expanding their response into perfectly emitting and absorbing modes. It is shown that the frequencies of these modes determine the shape of the reflection and transmission spectra in the same way that the positions of point-like charges determine the electric field around them. This helps to develop a visual interpretation of many resonant effects which occur due to overlapping resonances, and the Fano interference effect is considered as a basic example. This approach works naturally in the domain of complex frequencies and provides a systematic tool to analyze, optimize, and engineer the resonant properties of nanostructures for various applications.

I. INTRODUCTION

Plasmonic nanostructures and metamaterials offer unique abilities to engineer optical properties at subwavelength scales [1,2]. Arrays of split-ring resonators and fishnet structures provide strong magnetic resonances at optical frequencies [3]. Dolmen-like structures and oligomers enable tuning of the optical resonances [4–6] and observation of electromagnetically induced transparency [7] or absorption [8]. Arrays of holes in a metal film demonstrate strong Fano resonances which are very useful for filtering and sensing applications [9,10].

Numerical methods such as finite element [11,12], boundary element [13,14], and Fourier modal [15,16] are particularly efficient for modeling the aforementioned complex plasmonic metamaterials. However, interpreting the numerical results is not always straightforward because of the many different effects that appear simultaneously. Thus, it is desirable to have a semianalytical framework which can be built on the numerical data and can explain the results of the computations in a clear and systematic way. The existing approaches are often limited to the interplay of just two modes, commonly referred to as bright (radiative) and dark (nonradiative) modes [17–20]. Another difficulty is that these approaches rely on a large number of fitting parameters which cannot be extracted directly from the physical properties of the systems [21–23].

Here we provide a widely applicable framework to analyze, optimize, and engineer the resonant properties of nanostructures. It is based on the ability to expand the frequency response of nanostructures into a set of perfectly emitting and absorbing modes. These modes exist in the domain of complex frequencies, and we studied their properties by using the particles of spherical shape in our earlier paper [24]. Now we develop a special decomposition technique which allows us to remove many limitations of the previous theory and to apply it for arrays of nonspherical scatterers. Moreover, we show that the singularities created in the domain of complex frequencies by the perfectly emitting and absorbing modes have exactly the same type as the singularities created by positive and negative electric charges in two-dimensional (2D) space. This helps to build a useful analogy with electrostatics and to develop

a visual interpretation for many resonant effects which occur due to overlapping resonances.

II. DECOMPOSITION OF SCATTERING MATRIX

As a typical example of plasmonic metamaterial bearing Fano resonance features, we consider a planar array of dolmen-like metamaterial (Fig. 1). The periods of the elementary cell are made smaller than the wavelength of light to assure that the diffraction effects are suppressed for the plane-wave incidence. The reflected and transmitted waves of the zero order can be observed far from the structure, while all diffracted waves of higher orders are turned into evanescent waves which contribute only to the near field. In overall, this system can be considered as a black box with two input-output ports, or scattering channels.

When the structure has a mirror symmetry in the yz plane (or a similar one), incident waves with the electric or magnetic field directed along the y axis do not change their polarization after the scattering. The two independent polarizations can be considered separately, and in each case the system can be described by a scattering matrix $\mathbf{S}$. It has the dimensions 2×2 and links the amplitudes of the ingoing (u_+, v_+) and outgoing (u_-, v_-) plane waves as

$$\begin{pmatrix} u_- \\ v_- \end{pmatrix} = \mathbf{S} \begin{pmatrix} u_+ \\ v_+ \end{pmatrix}. \tag{1}$$

The components of the S matrix give the reflection R_p and transmission T_p coefficients for waves launched from the port p ("U" or "V"):

$$\mathbf{S} = \begin{bmatrix} R_\mathrm{U} & T_\mathrm{V} \\ T_\mathrm{U} & R_\mathrm{V} \end{bmatrix}. \tag{2}$$

The S matrix can be simplified further if the structure has a mirror symmetry in the xy plane, which is true for a large number of planar plasmonic structures including the dolmen-like structure shown in Fig. 1. The symmetry still allows an arbitrary profile of the scatterers in the xy plane and leaves enough flexibility for the design of resonant properties. As a consequence of the mirror symmetry, all modes of the structure can be divided into two groups [25]: even modes for which

---
[*]victor.grigoriev@fresnel.fr
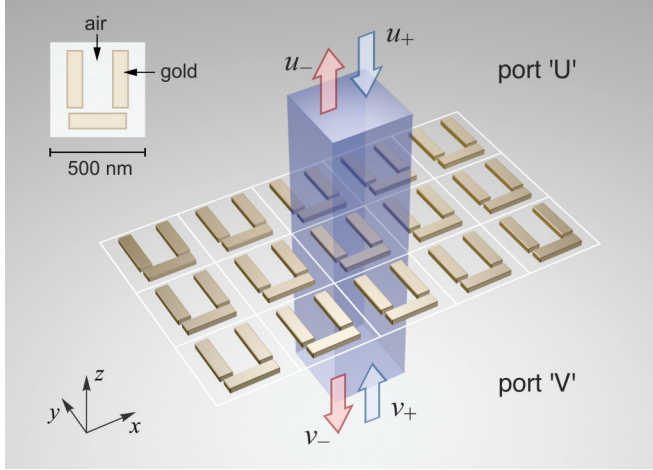
FIG. 1. (Color online) Schematic of a 2D grating composed of dolmen-like structures. The boundaries of elementary cells are highlighted in white, and the semitransparent box around the cell in the middle shows the abstract scattering channels. The periods of the grating are $a_x = a_y = 500$ nm. Each cell contains three bars of gold with dimensions $d_1 = 300$ nm $\times$ $d_2 = 80$ nm and thickness $d_z = 40$ nm. The gaps between bars in the same cell are $g_x = 160$ nm and $g_y = 30$ nm. The structure is surrounded by air, and the permittivity of the bars is described by the Drude model $\varepsilon(\omega) = 1 - \omega_p^2/(\omega^2 + i\Gamma\omega)$ with the parameters $\hbar\omega_p = 9.0$ eV and $\Gamma = 0.009\omega_p$ [7,17].

Eq. (1) can be rewritten as

$$\mathbf{S}\begin{pmatrix} 1 \\ 1 \end{pmatrix} = S_e \begin{pmatrix} 1 \\ 1 \end{pmatrix} \qquad (3)$$

and odd modes which satisfy

$$\mathbf{S}\begin{pmatrix} 1 \\ -1 \end{pmatrix} = -S_o \begin{pmatrix} 1 \\ -1 \end{pmatrix}. \qquad (4)$$

The eigenvalues S_e and S_o can be considered reflection coefficients for standing waves of even and odd symmetry [26].

The two solutions (3) and (4) are sufficient to perform the eigenvalue decomposition [27] of the S matrix at any frequency,

$$\mathbf{S} = \mathbf{C}\mathbf{S}_D\mathbf{C}^{-1}, \qquad (5)$$

where $\mathbf{S}_D$ is a diagonal matrix,

$$\mathbf{S}_D = \begin{bmatrix} S_e & 0 \\ 0 & -S_o \end{bmatrix}, \qquad (6)$$

and $\mathbf{C}$ is a conversion matrix built from the even and odd eigenvectors in Eqs. (3) and (4),

$$\mathbf{C} = \frac{1}{\sqrt{2}}\begin{bmatrix} 1 & 1 \\ 1 & -1 \end{bmatrix}. \qquad (7)$$

The reflection and transmission coefficients can be expressed in terms of the even and odd modes as

$$R = (S_e - S_o)/2, \qquad (8)$$

$$T = (S_e + S_o)/2, \qquad (9)$$

which can be obtained by writing Eq. (5) in the explicit form and comparing it with Eq. (2).

III. EMITTING AND ABSORBING MODES

Regardless of the even-odd symmetry, all modes of the structure can be of two types: perfectly emitting or perfectly absorbing [24]. They form a complete basis and satisfy the outgoing ($u_+ = v_+ = 0$) or ingoing ($u_- = v_- = 0$) boundary conditions, respectively. Since the input and output from the system are related by Eq. (1), such boundary conditions imply that the S matrix should be singular, with the determinants $|\mathbf{S}^{-1}(\omega_r^-)| = 0$ and $|\mathbf{S}(\omega_r^+)| = 0$ at the resonant frequencies of perfectly emitting ω_r^- and absorbing ω_r^+ modes, respectively.

The singularities of the S matrix can be linked to the singularities of its diagonal components by using the decomposition, (5)–(7), which gives $\det \mathbf{S} = -S_e S_o$. Therefore, the resonant frequencies $\omega_r^{\pm}$ correspond to the poles and zeros of either $S_e(\omega)$ or $S_o(\omega)$. It is known, however, that the poles and zeros of some function are fully sufficient to restore it anywhere in the complex plane. This follows from the Weierstrass factorization theorem [28], which can be written, for any diagonal component n ("e" or "o"), as

$$S_n(\omega) = A_n \exp(i B_n \omega) \prod_{r \in S_n} \frac{\omega - \omega_r^+}{\omega - \omega_r^-}. \qquad (10)$$

In this formula, A_n and B_n are constants, and the product is taken over all resonances which match the symmetry of S_n. The diagonal components have a number of properties which follow from the general physical requirements. For example, it can be proved that the constants A_n and B_n are real and that there are several symmetry relations between poles and zeros (see Appendixes A and B). Substitution of this formula into Eqs. (8) and (9) immediately gives the analytical formulas for the reflection and transmission spectra.

This approach deals directly with the resonances of the structure and does not require any fitting parameters, which simplifies the analysis of the spectra significantly. The dolmen-like structures shown in Fig. 1 can be considered as a typical example. The reflection spectrum for the normal incidence can be computed with the finite-element method and is given in Fig. 2. All frequencies are specified in normalized units so that $\omega_0 = 2\pi c/\lambda_0$ corresponds to the wavelength $\lambda_0 = 1$ μm and the energy of the photons $\hbar\omega_0 = 1.24$ eV. By solving an eigenvalue problem first with the outgoing boundary conditions and then with the ingoing ones, it is possible to extract the emitting and absorbing modes of the structure [24].

It turns out that there are only even modes in the frequency range of interest. Their resonant frequencies are $\omega_1^+ = (0.8485 + 0.0048i)\omega_0$, $\omega_2^+ = (1.0276 + 0.0744i)\omega_0$, $\omega_1^- = (0.8490 - 0.0297i)\omega_0$, and $\omega_2^- = (1.0258 - 0.1036i)\omega_0$. The field distributions of these modes reveal a quadrupolar ($\omega_1^{\pm}$) and dipolar ($\omega_2^{\pm}$) pattern (Fig. 2). The imaginary part of the resonant frequencies serves as a measure of the radiative or absorptive efficiency, and it is much smaller for the modes of quadrupolar pattern.

The constant A_e can be found by using the fact that in the limit of long wavelengths $S_e(0) = 1$. Substitution of the extracted resonances in Eq. (10) then gives $A_e = 1.0041$. The remaining constant B_e can be found by solving Eq. (10) with respect to B_e for any frequency in the middle of the spectra. The value of S_e at this intermediate point can be found directly from the reflection and transmission coefficients as
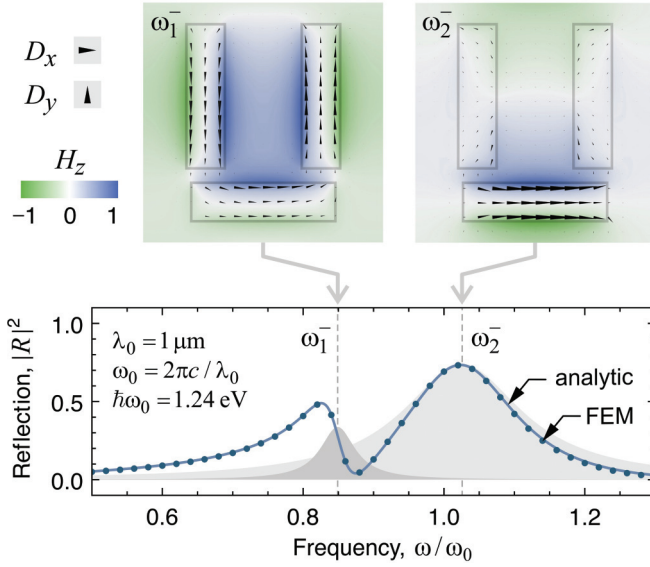
FIG. 2. (Color online) Reflection spectrum of the structure in Fig. 1. The normal incidence is considered, with the electric field polarized along the x axis. The results of the finite-element method are plotted as filled circles, while the results of the analytical formulas, (8) and (10), are shown as the solid line. Dashed lines indicate the positions of the emitting modes ω_1^- and ω_2^-. Their contributions to the spectrum are shown by contours in the background. Insets (top): Mode profiles in the plane $z = 0$.

$S_e = R + T$ according to Eqs. (8) and (9). This gives $B_e = 0.3350/\omega_0$. Similar calculations for odd modes show that $A_o = 1.0000$ and $B_o = -0.0126/\omega_0$. As such, the odd modes do not exist in the frequency range of interest, but there can be some tail created by the odd modes at higher frequencies, and it can be described as $S_o = A_o \exp(i B_o \omega)$.

Since all parameters for formulas (8) and (10) are known, they can be used to reconstruct the shape of the reflection spectrum. The agreement with the numerical data is very good over a broad range of frequencies (Fig. 2). Moreover, this approach works naturally in the domain of complex frequencies, and the analysis of the scattering spectra in the complex plane offers several benefits. It turns out that the interplay among different resonances can be explained in the same way as the interplay among point-like charges in electrostatics.

The analogy is due to the fact that the electrostatic field in the 2D case can be described by the complex potential of the form $\Phi(z) = -2 \sum_m q_m \ln(z - z_m)$, where the sum is taken over all charges q_m located at points $z_m = x_m + i y_m$ [29]. If all charges differ only in their sign $q_m^\pm = \pm q_0$, and the positive (negative) ones are located at the points z_m^+ (z_m^-), the complex potential can be rewritten as

$$\Phi(z) = -2 q_0 \ln \prod_m \frac{z - z_m^+}{z - z_m^-}, \qquad (11)$$

which strongly resembles the factorization theorem, (10). Therefore, the poles and zeros can be viewed as point-like charges of positive and negative sign, and it is possible to apply the well-developed formalism of electrostatics to analyze the scattering spectra.
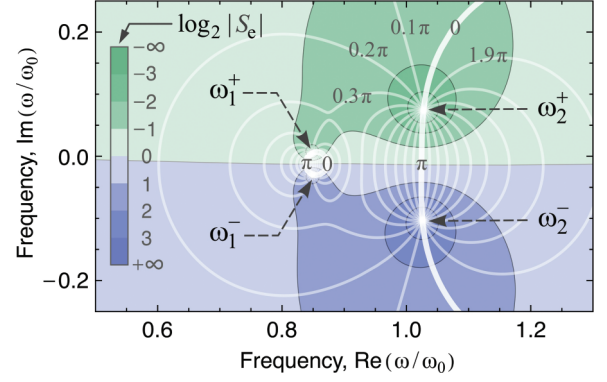
FIG. 3. (Color online) $S_e(\omega)$ component as a function of complex frequency for the structure in Fig. 1. The positions of poles ω_r^- and zeros ω_r^+ are labeled. Contours of blue and green shades show the absolute value of S_e on a logarithmic scale. White contour lines give the phase of S_e in steps of π for thick lines and $\pi/10$ for thin lines.

First, this means that the scattering spectra $S_n(\omega) = |S_n| \exp(i \varphi_n)$ can be visualized in terms of the equipotential contours (amplitude contours, $|S_n| = $ const) and electric-field lines (phase lines, $\varphi_n = $ const). An example of such visualization is given in Fig. 3, and it shows explicitly how the positions of poles and zeros affect the shape of the spectra for real frequencies. The density of the phase lines describes the steepness of the resonances in the reflection spectrum. For example, it can be noted that the pair of pole and zero $\omega_1^\pm$ is situated closer to the real axis than $\omega_2^\pm$, and it produces sharper variations in the reflection spectrum (Fig. 2). It can be proved that the density of the phase lines $d\varphi_n/d\omega$ (the number of phase lines crossing a given interval of frequencies) is actually proportional to the photonic density of states, and it tends to infinity near the poles and zeros [30,31].

IV. FANO RESONANCES

A large number of resonant effects (electromagnetically induced transparency, absorption, etc.) can be explained just as a result of different superpositions created by multiple point-like singularities. The simplest and most important example of such effects is the Fano interference, which creates resonances of an asymmetric shape [5,6]. The use of perfectly emitting and absorbing modes helps to develop a novel interpretation of this effect. In fact, each isolated pair of pole ω_r and zero ω_r^* can produce a Fano shape in the spectrum. If this pair belongs to even modes, Eq. (10) can be simplified and the diagonal components of the S matrix can be approximated as

$$S_e(\omega) \approx \exp(i \varphi_e) \frac{\omega - \omega_r^*}{\omega - \omega_r}, \qquad (12)$$

$$S_o(\omega) \approx \exp(i \varphi_o), \qquad (13)$$

where φ_e and φ_o are constants which represent a combined phase created in the vicinity of the selected pair by all other poles and zeros. These smoothly varying phases play the same role as the continuum states in the classical Fano theory, and the discrete state corresponds to the pole-zero term. By introducing the normalized frequency detuning $\xi = [\mathrm{Re}(\omega_r) - \omega]/\mathrm{Im}(\omega_r)$ and the phase mismatch $\Delta\varphi = \varphi_e - \varphi_o$,

the reflection coefficient, (8), can be represented as

$$|R|^2 = \frac{1}{4}\left|e^{i\Delta\varphi}\frac{\xi - i}{\xi + i} - 1\right|^2 = \frac{|\text{Im}[e^{i\Delta\varphi/2}(\xi - i)]|^2}{\xi^2 + 1}. \quad (14)$$

The latter expression leads to the formula

$$|R|^2 = \frac{[\xi\sin(\Delta\varphi/2) - \cos(\Delta\varphi/2)]^2}{\xi^2 + 1}, \quad (15)$$

which coincides with the classical formula derived by Fano [32] for the scattering cross section $\sigma(\xi)$:

$$\sigma(\xi) = \frac{(\xi + q)^2}{\xi^2 + 1}. \quad (16)$$

The asymmetry parameter q controls the shape of the spectrum, and comparison of Eqs. (15) and (16) gives an explicit formula for it in terms of interference effects between even and odd modes, $q = -\cot(\Delta\varphi/2)$. Moreover, it is possible to develop a graphical interpretation for the Fano effect (Fig. 4), and the analysis of the simplified example provides many clues for interpreting more complex cases as in Fig. 3. In fact, the resonances $\omega_1^{\pm}$ in Fig. 3 can be considered as an isolated pole-zero pair, and the phase mismatch can be estimated as $\Delta\varphi = 0.3\,\pi$. The same value was used in the model in Fig. 4, so that it can reproduce a part of the reflection spectrum around $\omega_1^{\pm}$ in Fig. 2.
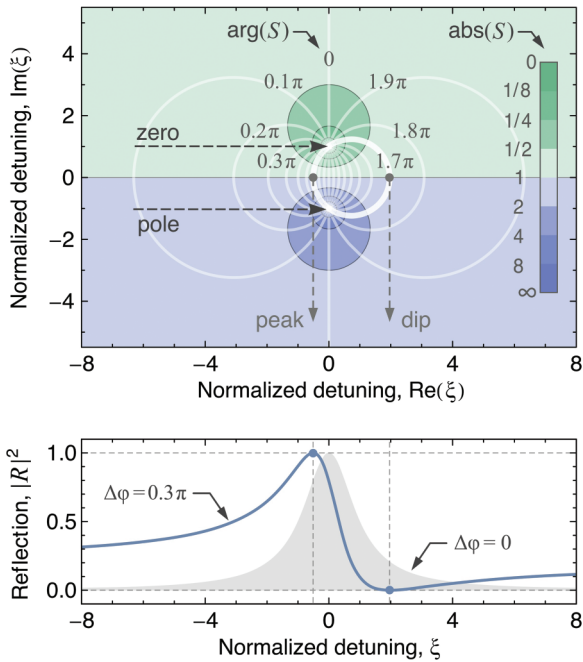
FIG. 4. (Color online) Contour map of the scattering term $S = (\xi - i)/(\xi + i)$ created by an isolated pair of pole and zero. The use of normalized units assures that every two contours of constant phase $\arg(S) = C$ and $\arg(S) = C + \pi$ form a circle which always passes through the pole and zero. The positions of the dip and peak in the reflection spectrum $|R|^2 = |(Se^{i\Delta\varphi} - 1)/2|^2$ can be predicted as the intersection points of the circle $C = -\Delta\varphi$ with the real axis. One such circle, for $\Delta\varphi = 0.3\pi$, is shown with a greater thickness. When the phase mismatch between even and odd modes disappears, $\Delta\varphi = 0$, the spectrum acquires a Lorentzian shape.

The contour maps in Fig. 4 clearly show that the positions of the dip ξ_d and peak ξ_p in the spectrum are related to each other. They can be predicted as the intersection points of the real axis with a circle passing through the pole and zero. The distance between the peak and the dip $\xi_p - \xi_d = q + q^{-1} = -2/\sin\Delta\varphi$ coincides with the diameter of the circle. Therefore, the minimal possible separation between them is $|\xi_p - \xi_d| = 2$. It occurs when $\Delta\varphi = \pm\pi/2$ and puts the upper limit on the steepness of the Fano profiles. The conversion to normal frequencies gives the formula for the distance between peak and dip $\omega_p - \omega_d = -\text{Re}(\omega_r)/(Q_r\sin\Delta\varphi)$, where $Q_r = \text{Re}(\omega_r)/[2\,\text{Im}(\omega_r)]$ is the quality factor of the resonance at ω_r. The sign of $\Delta\varphi$ determines the order in which the dip and peak appear in the spectrum and, as a consequence, the type of dispersion: normal and anomalous. The Lorenzian shape of the spectrum is obtained when $\Delta\varphi = 0$ and corresponds to the situation when the dip is shifted to infinity so that the spectrum acquires a symmetric shape with the peak in the center. If $\Delta\varphi = \pi$, the positions of the dip and peak can be inverted, and in this case the shape of the spectrum becomes complementary to the Lorentzian one.

V. CONCLUSIONS

To summarize, we developed a semianalytical approach to explain the scattering spectra of plasmonic nanostructures. Our approach takes full advantage of the spectral decomposition over an orthogonal basis formed by the eigenmodes of the photonic structure. We demonstrate that the frequencies of these modes fully determine the complex features of the reflection and transmission spectra over an arbitrarily broad range of frequencies, and we show explicitly how the interplay between the resonant frequencies produces different resonant effects. Importantly, our approach considers the photonic device as an ensemble and is no longer limited by the number of fitting parameters that must be taken into account. This offers a new point of view regarding the resonant properties of nanostructures and significantly simplifies the analysis of their spectra.

APPENDIX A: TIME-REVERSAL SYMMETRY

All physical structures have the important property that the response to an excitation described by a real function must be a real function as well. This also applies to the Green's function $G(t)$, which is defined as the response to an infinitely short excitation. Since the diagonal components of the S matrix can be expressed as the Fourier transform of a diagonalized

Green's function,

$$S(\omega) = \int_{-\infty}^{+\infty} G(t)\exp(-i\omega t)dt, \tag{A1}$$

and the Green's function is real $G(t) = [G(t)]^*$, Eq. (A1) can be transformed as

$$[S(\omega)]^* = \int_{-\infty}^{+\infty} G(t)\exp(i\omega^* t)dt. \tag{A2}$$

Comparison of Eqs. (A1) and (A2) leads to the relation

$$S(\omega) = [S(-\omega^*)]^*. \tag{A3}$$

This is known as the time-reversal symmetry and is valid for both lossless and lossy structures [33,34]. Note that Eq. (A3) is often simplified to $S(\omega) = [S(-\omega)]^*$, which is less general and can be used only for real frequencies and lossless structures.

Substitution of the Weierstrass factorization theorem,

$$S(\omega) = A\exp(iB\omega)\prod_r \frac{\omega - \omega_r^+}{\omega - \omega_r^-}, \tag{A4}$$

into the right-hand side of Eq. (A3) gives

$$S(\omega) = A^*\exp(iB^*\omega)\prod_r \frac{\omega + (\omega_r^+)^*}{\omega + (\omega_r^-)^*}. \tag{A5}$$

Similarly to the expansions into Taylor series, the Weierstrass factorization is unique so that a term-by-term comparison of Eqs. (A4) and (A5) can be performed. This proves that the parameters A and B are real. Moreover, it also follows from the comparison that the poles and zeros exist in pairs $\{\omega_r^\pm, -(\omega_r^\pm)^*\}$ which are mirror symmetric with respect to the imaginary axis.

APPENDIX B: ENERGY CONSERVATION

If a structure is lossless, the scattered waves carry the same amount of energy as the incident ones. This leads to the unitarity of the S matrix for all real frequencies [33,34] and can be written as

$$[\mathbf{S}(\omega)]^\dagger \mathbf{S}(\omega) = \mathbf{I}. \tag{B1}$$

If the S matrix is diagonal, Eq. (B1) applies for each scattering channel independently, which gives

$$|S(\omega)|^2 = 1 \tag{B2}$$

and, after analytical continuation to the entire complex plane,

$$S(\omega)[S(\omega^*)]^* = 1. \tag{B3}$$

Since $S(\omega) = a_{\text{out}}/a_{\text{in}}$, Eq. (B2) simply states that the amplitudes of the outgoing a_{out} and incoming a_{in} waves are equal.

It is convenient to rewrite the energy conservation, (B3), in the form

$$S(\omega) = 1/[S(\omega^*)]^*. \tag{B4}$$

The substitution of the Weierstrass factorization theorem, (A4), into the right-hand side of Eq. (B4) gives

$$S(\omega) = \frac{\exp(iB^*\omega)}{A^*}\prod_r \frac{\omega - (\omega_r^-)^*}{\omega - (\omega_r^+)^*}. \tag{B5}$$

A term-by-term comparison of Eqs. (A4) and (B5) then shows that $|A|^2 = 1$ and $B = B^*$. Moreover, it also follows from the comparison that the poles and zeros are not independent and can be related to each other as $\omega_r^+ = (\omega_r^-)^*$. Therefore, each pole and zero form a pair which is mirror symmetric with respect to the real axis.

When the structure is lossy but remains passive (without gain), Eq. (B2) should be modified to

$$|S(\omega)|^2 < 1, \tag{B6}$$

because the amplitude of the outgoing wave must be lower than the amplitude of the incoming one. For mirror-symmetric structures, the reflection R and transmission T spectra can be described in terms of the even S_{e} and odd S_{o} modes as

$$R = (S_{\text{e}} - S_{\text{o}})/2, \tag{B7}$$

$$T = (S_{\text{e}} + S_{\text{o}})/2. \tag{B8}$$

It can be checked that

$$|R|^2 + |T|^2 = (|S_{\text{e}}|^2 + |S_{\text{o}}|^2)/2 < 1. \tag{B9}$$

Therefore, the energy conservation for the even and odd scattering channels ensures energy conservation for plane-wave incidence.

[1] S. Enoch and N. Bonod, *Plasmonics: From Basics to Advanced Topics* (Springer, Berlin, 2012).

[2] L. Solymar and E. Shamonina, *Waves in Metamaterials* (Oxford University Press, Oxford, 2009).

[3] C. M. Soukoulis, S. Linden, and M. Wegener, Science **315**, 47 (2007).

[4] J. A. Fan, C. Wu, K. Bao, J. Bao, R. Bardhan, N. J. Halas, V. N. Manoharan, P. Nordlander, G. Shvets, and F. Capasso, Science **328**, 1135 (2010).

[5] B. Luk'yanchuk, N. I. Zheludev, S. A. Maier, N. J. Halas, P. Nordlander, H. Giessen, and C. T. Chong, Nat. Mater. **9**, 707 (2010).

[6] M. Rahmani, B. Luk'yanchuk, and M. Hong, Laser Photon. Rev. **7**, 329 (2013).

[7] N. Liu, T. Weiss, M. Mesch, L. Langguth, U. Eigenthaler, M. Hirscher, C. Sonnichsen, and H. Giessen, Nano Lett. **10**, 1103 (2010).

[8] R. Taubert, M. Hentschel, J. Kastel, and H. Giessen, Nano Lett. **12**, 1367 (2012).

[9] F. J. Garcia de Abajo, Rev. Mod. Phys. **79**, 1267 (2007).

[10] C. Genet, M. P. van Exter, and J. Woerdman, Opt. Commun. **225**, 331 (2003).

[11] G. Demesy, F. Zolla, A. Nicolet, and M. Commandre, Opt. Lett. **34**, 2216 (2009).

[12] Y. Zhu and A. C. Cangellaris, *Multigrid Finite Element Methods for Electromagnetic Field Modeling* (Wiley, Hoboken, NJ, 2006).

[13] B. Gallinet, A. M. Kern, and O. J. F. Martin, J. Opt. Soc. Am. A **27**, 2261 (2010).

[14] G. Boudarham and M. Kociak, Phys. Rev. B **85**, 245447 (2012).

[15] V. Liu and S. Fan, Comput. Phys. Commun. **183**, 2233 (2012).

[16] H. Kim, J. Park, and B. Lee, *Fourier Modal Method and Its Applications in Computational Nanophotonics* (CRC Press, Boca Raton, FL, 2012).

[17] B. Gallinet and O. J. F. Martin, Phys. Rev. B **83**, 235427 (2011).

[18] B. Gallinet and O. J. F. Martin, ACS Nano **5**, 8999 (2011).

[19] V. Giannini, Y. Francescato, H. Amrania, C. C. Phillips, and S. A. Maier, Nano Lett. **11**, 2835 (2011).

[20] M. Hentschel, D. Dregely, R. Vogelgesang, H. Giessen, and N. Liu, ACS Nano **5**, 2042 (2011).

[21] T. J. Davis, M. Hentschel, N. Liu, and H. Giessen, ACS Nano **6**, 1291 (2012).

[22] S. Zhang, D. A. Genov, Y. Wang, M. Liu, and X. Zhang, Phys. Rev. Lett. **101**, 047401 (2008).

[23] S. Mukherjee, H. Sobhani, J. B. Lassiter, R. Bardhan, P. Nordlander, and N. J. Halas, Nano Lett. **10**, 2694 (2010).

[24] V. Grigoriev, A. Tahri, S. Varault, B. Rolly, B. Stout, J. Wenger, and N. Bonod, Phys. Rev. A **88**, 011803(R) (2013).

[25] K. Sakoda, *Optical Properties of Photonic Crystals*, 2nd ed., Springer Series in Optical Sciences (Springer, Berlin, 2004).

[26] V. Grigoriev and F. Biancalana, J. Opt. Soc. Am. B **28**, 2165 (2011).

[27] C. D. Meyer, *Matrix Analysis and Applied Linear Algebra* (SIAM, Philadelphia, 2000).

[28] G. B. Arfken and H. J. Weber, *Mathematical Methods for Physicists*, 5th ed. (Academic Press, San Diego, CA, 2001).

[29] W. R. Smythe, *Static and Dynamic Electricity*, 3rd ed. (McGraw–Hill, New York, 1967).

[30] V. Grigoriev and F. Biancalana, Opt. Lett. **36**, 3774 (2011).

[31] G. D'Aguanno, N. Mattiucci, M. Scalora, M. J. Bloemer, and A. M. Zheltikov, Phys. Rev. E **70**, 016612 (2004).

[32] U. Fano, Phys. Rev. **124**, 1866 (1961).

[33] H. M. Nussenzveig, *Causality and Dispersion Relations* (Academic Press, New York, 1972).

[34] R. G. Newton, *Scattering Theory of Waves and Particles*, 2nd ed. (Springer, New York, 1982).